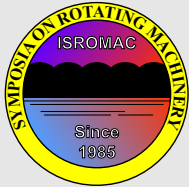


Effect of non-uniform flexibility on hydrodynamic performance of pitching propulsors

Samane Zeyghami^{1*}, Keith W. Moored¹



ISROMAC 2017

International
Symposium on
Transport Phenomena
and
Dynamics of Rotating
Machinery

Maui, Hawaii

December 16-21, 2017

Abstract

Many aquatic animals propel themselves efficiently through water by oscillating flexible fins. These fins are, however, not homogeneously flexible, but instead their flexural stiffness varies along their chord and span. Here, we developed a low order model of these functionally-graded materials where the chordwise flexibility of the foil is modeled by one or two torsional springs along the chordline. The torsional spring structural model is then strongly coupled to a boundary element fluid model to simulate the fluid-structure interactions. We show that the *effective flexibility* of the combined fluid-structure system scales with the ratio of the added mass forces acting on the passive portion of the foil and the elastic forces defined by the torsional spring hinge. We further detail the dependency of the propulsive performance on the flexibility and location of the single torsional spring for a foil that is actively pitching about its leading edge. Our results show that increasing the flexion ratio by moving the spring away from the leading edge leads to enhanced propulsive efficiency, but compromises the thrust production. Proper combination of two flexible hinges, however, can result in a gain in both the thrust production and propulsive efficiency.

Keywords

Nonuniform flexibility – Unsteady propulsion – Propulsive performance – Pitching – Bending patterns

¹ Department of Mechanical Engineering and Mechanics, Lehigh University, Bethlehem, USA

*Corresponding author: saz316@lehigh.edu

INTRODUCTION

Flying and swimming animals propel themselves rapidly and efficiently through a fluid using flexible propulsors. A substantial line of work has already confirmed that flexible propulsors are advantageous to rigid ones in aquatic locomotion, specifically with regard to propulsive efficiency [1, 2, 3, 4]. Some have argued that the interactions between the fluid and the structure deforms the foil in the direction of the fluid. These deformations lead to curvature-induced thrust increases [5] as well as a favorable phase lag between the pitching and heaving motions of the foil which in return enhances propulsive efficiency [6, 7]. In addition, the occurrence of resonance is argued to play an important role in enhancing propulsive performance of flexible foils. Previous studies have shown that the efficiency is maximized at or near the resonance frequency of the combined fluid-structure system [8, 4]. The resonance frequency of the combined system is a function of the inertial properties of the structure as well as the added mass arising from inertia of the fluid. However, when the flexibility is variable along the chord, the scaling of the resonance frequency of the fluid-structure system is non-trivial, a topic that we will attend to in the present study.

The propulsive appendages of swimming and flying animals are made of functionally-graded materials where the flexibility varies both along the chord and span. In fact, Combes and Daniel [9] measured the flexural stiffness of several insect wings and found that it declines sharply from the wing base to wing tip, in the spanwise direction, and

from the leading edge to the trailing edge, in the chordwise direction. Similarly, the flexibility of the propulsive surfaces of swimming animals (such as fluke, fin and tail) appear to be non-uniform and decline from the leading to trailing edge and from the center to the edges [10, 11, 12]. Inspired by these observations, a number of recent studies have suggested that the distribution of the flexibility along the foil, in addition to its overall flexibility, may play an important role in enhancing the propulsive performance. Comparing different distributions of flexibility along a two dimensional thin foil undergoing small amplitude heaving motions, Moore [13] has suggested that the concentration of the flexibility at the leading edge enhances thrust production. In another study, Riggs et al. [14] have tested the thrust production of a flexible fin with a standard NACA0012 cross-sectional shape alongside fins with a stiffness profiles mimicking that of a Pumpkinseed Sunfish. They showed that bio-mimetic fins generate more thrust regardless of the overall stiffness of the fin, showing that the performance improvement is due to the stiffness profile itself and not the flexibility alone. Similar conclusions were found by [12] in an experimental study on the propulsive performance of robotic fins with variable chordwise flexibility. They found that fins with variable flexibility outperformed the fins with uniform flexibility with regard to both thrust production and propulsive efficiency.

Here we aim to probe the effect of the distribution of flexibility on the propulsive performance of a pitching foil by separating the effect of the overall flexibility of a pitching foil from that of its bending pattern. We model the chord-

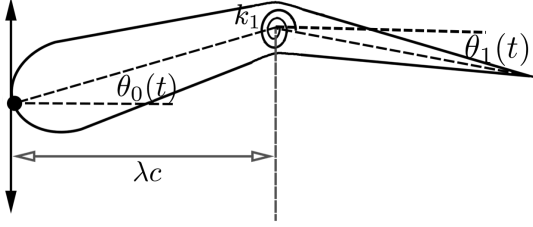


Figure 1. Schematic of the model for a single spring.

wise flexibility of the foil with a series of torsional springs with varying flexibility. The effect of the bending patterns is modeled via changing the location of the spring along the chord. First, we investigate the propulsive performance of a pitching foil with a single flexible joint. We detail the effect of both the overall flexibility and the bending pattern of the foil. Next, we repeat our numerical experiment on a pitching foil with two flexible joints. This time the location of the flexible joints are fixed but the distribution of the flexibility is varied. This study is a primary step toward understanding the role the functionally graded materials on the propulsive performance. Results of this study can also inspire design of innovative and non-traditional propulsors.

1. PROBLEM DEFINITION

All the numerical experiments are performed on a two-dimensional foil where the leading edge of the foil is actively pitching with a peak-to-peak amplitude of $2\theta_0 = 10^\circ$. There are either one or two flexible joints along the chord modeled by torsional springs (figure 1). The distance of the flexible joint from the leading edge, normalized by the chord length, is quantified by the flexion ratio, λ . The flapping frequency and swimming velocity are kept constant across these simulations at 2.87 Hz and 0.1 m/s resulting in a reduced frequency of $k = 2.87$ (defined as $k = \frac{f c}{U}$) and a Strouhal number (defined as $St = \frac{f A}{U}$) of 0.5. This St is defined for a rigid foil without a flexible joint. However, the real St of the flow is an output of the system and varies with the trailing edge amplitude, which itself is a function of the flexibility and flexion ratio.

For materials with similar densities as that of the surrounding fluid (in the present study $\rho_s = \rho$), the flexibility of the combined fluid-structure system is a function of the added mass forces of the fluid and the elastic forces of the structure. We define Π_k as the ratio of these forces which characterizes the *effective flexibility* of the combined fluid-structure system.

$$\Pi_k = (1 - \lambda^2) \sqrt{\frac{\rho c^4 f^2}{k}} \quad (1)$$

where ρ , f , c , and k respectively are the fluid density, pitching frequency, chord length, and the spring stiffness. The numerator is the added mass force represented as a cylinder of fluid with a diameter equal to length of the passive portion

of the foil multiplied by a characteristic acceleration. Note that changing Π_k is equivalent to changing the resonance frequency of the system.

Both flexibility and flexion ratio are changed and their effect on the propulsive performance is detailed. The performance is analyzed using thrust and power coefficients as well the propulsive efficiency which are defined below.

$$C_t = \frac{T}{0.5\rho U^2 bc}, \quad C_p = \frac{P}{0.5\rho U^3 bc} \quad (2)$$

where T , and P are the thrust and input power. b is the span length that is set to 1. Alternatively, we normalized thrust and power with trailing edge velocity as defined in eqn. 3. Note that the trailing edge amplitude is an output of a flexible foil system.

$$C_t' = \frac{T}{0.5\rho A^2 f^2 bc}, \quad C_p' = \frac{P}{0.5\rho U A^2 f^2 bc} \quad (3)$$

where A is the trailing edge amplitude.

2. NUMERICAL METHODS

The flow over the foil is modeled using a two-dimensional potential flow method in which the flow is assumed to be irrotational, incompressible and inviscid. We follow [15] and [16], in that the general solution to the potential flow problem is reduced to finding a distribution of doublets and sources on the foil surface and in the wake that satisfies no flux boundary condition on the body at each time step. Constant strength source and doublet line elements are distributed over the body and the wake. Each body boundary element is assigned a collocation point which is shifted a small distance under the body surface (here 1% of the local thickness of the body). The constant potential Dirichlet condition is enforced at the collocation points to ensure a no flux boundary condition on the body surface. Additionally, at each time step a wake boundary element is shed with a strength that is set by applying an explicit Kutta condition, where the vorticity at the trailing edge is set to zero [17, 18, 19]. A wake rollup algorithm is employed to ensure that the wake does not support any force. The wake elements advect by the local velocity at the wake panel edge points. During the wake rollup the point vortices, representing the ends of the wake doublet elements, must be de-singularized for numerical stability of the solution [20]. To do so, at a small cutoff radius of $\epsilon = 0.05c$, the irrotational induced velocities from the point vortices are replaced by a rotational Rankine core model. The tangential perturbation velocity component is calculated by local differentiation of the perturbation potential. Finally, the pressure acting on the body is found via applying the unsteady Bernoulli equation. More details can be found in [15, 21, 22].

The structural flexibility is modeled via torsional springs which connect the structural mesh elements together. The kinematics of the leading structural element is always prescribed. Equation 4 governs the dynamics of the passive

structural elements.

$$I\ddot{\Theta} + C\dot{\Theta} + C\Theta = N_f + N_i + N_h \quad (4)$$

where N_f is the hydrodynamic moment exerted about the joint location. N_i is the inertial moment due to the translational velocity of the center of mass of the corresponding element. N_h is the moment exerted by the forces at the joint which keep the elements together. I is the matrix of moments of inertia about the joint points. K and C are the matrices of the structural stiffness and damping, respectively. Θ is a vector containing the orientation of the passive elements. For a foil with two flexible joints we have:

$$I \equiv \begin{bmatrix} I_1 & 0 \\ 0 & I_2 \end{bmatrix} \quad K \equiv \begin{bmatrix} k_1 + k_2 & -k_2 \\ -k_1 & k_2 \end{bmatrix} \quad C \equiv \begin{bmatrix} c_1 + c_2 & -c_2 \\ -c_1 & c_2 \end{bmatrix} \quad (5)$$

where I_i is the moment of inertia of the i^{th} element. c_i and k_i are the structural damping and the stiffness of the spring attached to the leading edge of the i^{th} element.

To solve the fluid-structure interaction problem, equation 4 is discretized in time, using the trapezoidal rule (equations 6 and 7), and solved within each small time step via a strong coupling between the fluid and structural solvers which is accelerated by the Aitken method. To improve the convergence properties of the solver, while keeping its efficiency, we use two different time step sizes Δt and Δt_s for the fluid and structure solvers, respectively, where $\Delta t_s = \frac{\Delta t}{N_s}$. N_s is set to 100 in the present simulations.

$$\hat{\Theta}^{m+1} = \hat{\Theta}^m + \frac{1}{2}(\dot{\hat{\Theta}}^m + \dot{\hat{\Theta}}^{m+1})\Delta t_s \quad (6)$$

$$\dot{\hat{\Theta}}^{m+1} = \dot{\hat{\Theta}}^m + \frac{1}{2}(\ddot{\hat{\Theta}}^m + \ddot{\hat{\Theta}}^{m+1})\Delta t_s \quad (7)$$

where superscripts m and $m + 1$ represent the values at times t_s^m and t_s^{m+1} , respectively. \hat{x} represents any variable x within the structure solver. Substituting equation 7 into equation 6 and solving for $\ddot{\Theta}^{m+1}$ we get:

$$\ddot{\Theta}^{m+1} = \left(\frac{2}{\Delta t_s}\right)^2(\hat{\Theta}^{m+1} - \hat{\Theta}^m) - \left(\frac{4}{\Delta t_s}\right)\dot{\hat{\Theta}}^m - \ddot{\Theta}^m \quad (8)$$

Similarly, equation 6 can be rearranged to get an expression for $\dot{\hat{\Theta}}^{m+1}$ as a function of $\hat{\Theta}$:

$$\dot{\hat{\Theta}}^{m+1} = \frac{2}{\Delta t_s}(\hat{\Theta}^{m+1} - \hat{\Theta}^m) - \dot{\hat{\Theta}}^m \quad (9)$$

Where the right hand sides of both equations 8 and 9 are known from the previous iteration.

Substituting equations 9 and 8 into 4, we can rewrite the governing equations as a linear, but coupled, system of equations as follows:

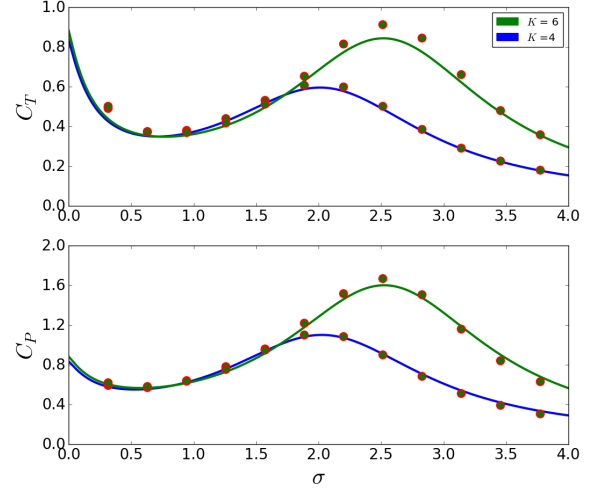


Figure 2. Analytical solutions for thrust and power coefficient as a function of reduced frequency, for two different non-dimensional spring stiffnesses, are shown with solid lines. These solutions are taken from [23]. Closed circles are the solutions calculated by the present numerical method.

$$\begin{aligned} A\hat{\Theta}^{m+1} &= \hat{b}^m \\ A &= K + \left(\frac{2}{\Delta t_s}\right)^2 I + \left(\frac{2}{\Delta t_s}\right)C \\ \hat{b}^m &= \left(\frac{2}{\Delta t_s}\right)^2 I\hat{\Theta}^m + \left(\frac{4}{\Delta t_s}\right)I\dot{\hat{\Theta}}^m + I\ddot{\hat{\Theta}}^m + \left(\frac{2}{\Delta t_s}\right)C\hat{\Theta}^m \\ &\quad + C\dot{\hat{\Theta}}^m + \hat{N}_i^m + \hat{N}_f^m + \hat{N}_h^m \end{aligned} \quad (10)$$

Equation 10 together with 6 and 7 form a complete set of equations for the structure. The set of structure equations are first initialized by the known solution from the previous time step (of the fluid's solver) and then iterated N_s times to advance the solution as much as Δt .

To improve convergence, equation 10 is uncoupled by employing a Gauss-Seidel formulation where the newly obtained solution for the orientation of the first element is used to obtain the solution for the second element at each time step t_s .

The Aitken acceleration method is commonly used in the numerical simulation of fluid-structure interactions and is proven to be sufficiently simple and efficient [24, 25, 26]. This method uses the values from the two previous iterations to correct the new solution. We employ Aitken's method to advance the solution in the fluid's solver based on the residual calculated in the previous two iterations. The residual is calculated as the difference in the solution obtained in the structure and the fluid solvers, $\vec{r}_i = \hat{\Theta}_i - \Theta_i$, where Θ_i is a vector representing the orientation of the neutral axis of the foil in the fluid solver.

The solution to the coupled fluid-structure system at each

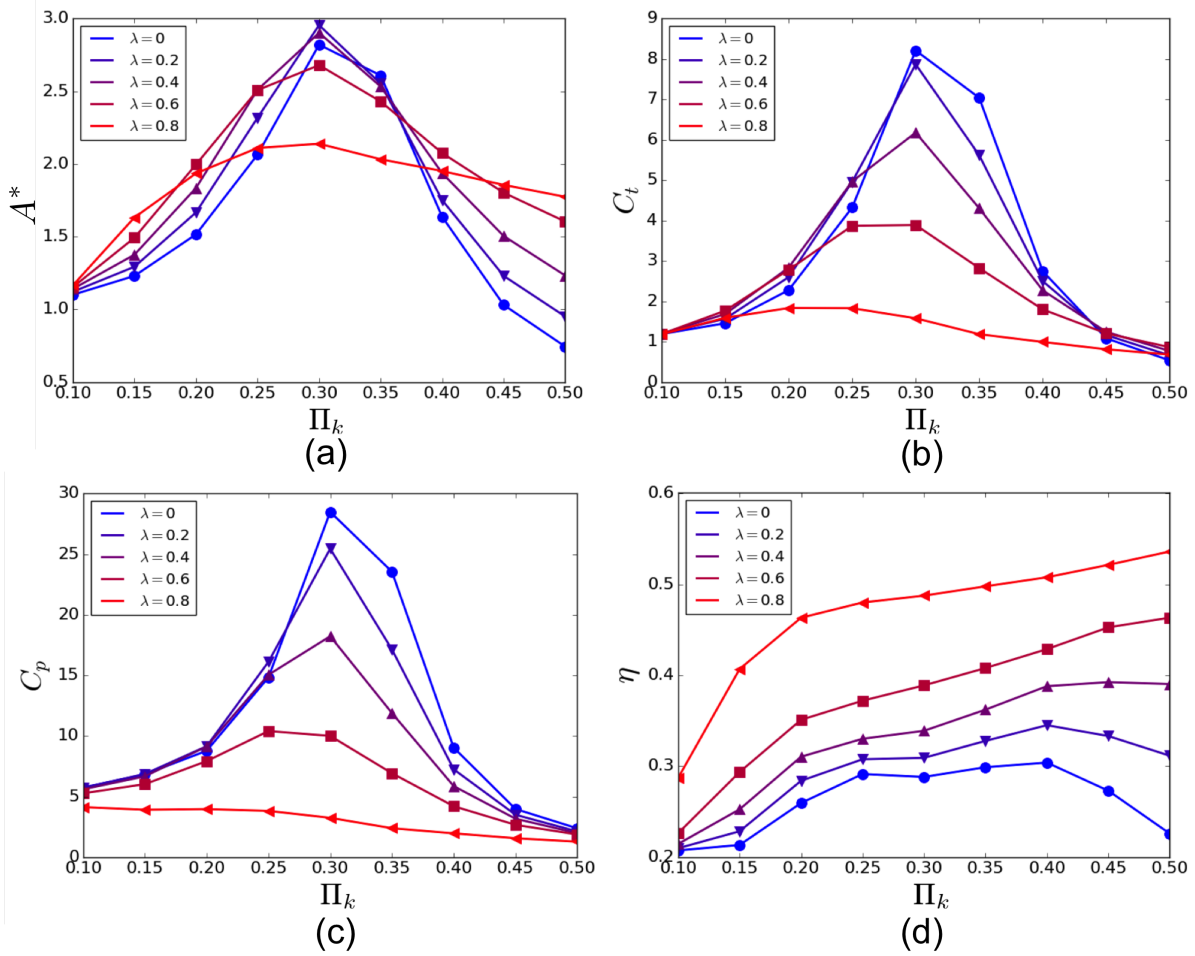


Figure 3. (a) Trailing edge amplitude, (b) thrust coefficient, (c) power coefficient, and (d) efficiency as a function of Π_k .

time step $t_n = n\Delta t$ is obtained by following the algorithm below:

1. $i = 0$, $r_0 = 1$, $\tilde{\Theta}_0 = \Theta_{n-1}$, $\dot{\tilde{\Theta}}_0 = \dot{\Theta}_{n-1}$, $\ddot{\tilde{\Theta}}_0 = \ddot{\Theta}_{n-1}$, and $\omega_0 = 1e - 2$
2. While $\|r_i\| > \delta$
 - (a) $i = i + 1$
 - (b) if $i > 1$ modify the solution; $\tilde{\Theta}_i = \tilde{\Theta}_{i-1} + \omega_{i-1}r_{i-1}$
 - (c) Calculate the location of the neutral axis of the foil in the fluid solver via known values of the leading element and passive elements.
 - (d) Calculate the position and velocity of the fluid panels on the foil surface.
 - (e) Calculate fluid forces and moments.
 - (f) Solve the solid deformations; $\hat{\Theta}_i$, $\dot{\hat{\Theta}}_i$, and $\ddot{\hat{\Theta}}_i$ using equations 10, 8, and 7
 - (g) Calculate the residual, $r_i = \hat{\Theta}_i - \tilde{\Theta}_i$
 - (h) Calculate Aitken Acceleration factor; if $i < 3$, $\omega_i = \omega_0$ else, $\omega_i = \omega_{i-1} \frac{\tilde{r}_{i-1}(\tilde{r}_{i-1} - \tilde{r}_i)}{\|\tilde{r}_{i-1} - \tilde{r}_i\|^2}$

3. Update the solution for time t_n ; $\Theta_n = \tilde{\Theta}_i$, $\dot{\Theta}_n = \dot{\tilde{\Theta}}_i$, and $\ddot{\Theta}_n = \ddot{\tilde{\Theta}}_i$

where δ is set to 10^{-8} . When the solution converges within the n^{th} time step, we set $n = n + 1$ and repeat the steps above to solve for the next time step.

2.1 Validation

We tested the accuracy of our numerical model by comparing our results against the analytical results presented in [23] for a two dimensional thin foil with a torsional spring at the leading edge. A small amplitude (harmonic) heaving motion is enforced at the leading edge. The foil passively pitches about the leading edge due to the action of fluid, inertial, and elastic forces. We compared both the cycle-averaged thrust and the cycle-averaged power with the analytical solution. Results are shown in Figure 2.

3. RESULTS AND DISCUSSION

3.1 Single flexible joint

Figure 3a shows the non-dimensional trailing edge amplitude, $A^* = \frac{A}{A_{rigid}}$, as function of effective flexibility for five differ-

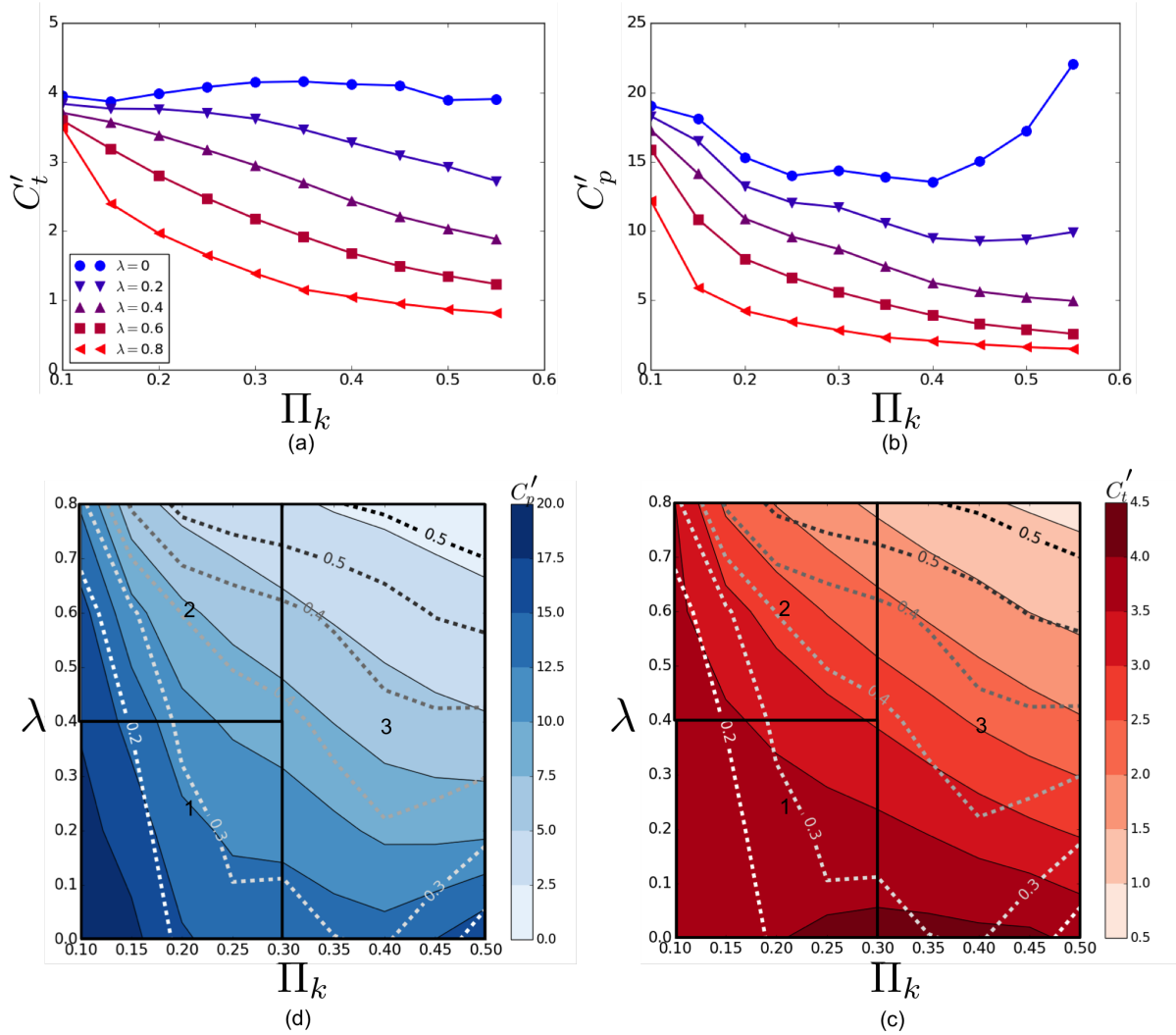


Figure 4. Variation of thrust (a) and power (b) coefficients, C'_t and C'_p , defined by equation 3 with Π_k . Contours of C'_t and C'_p in $\lambda - \Pi_k$ plane. Dotted lines are the contours of propulsive efficiency.

ent flexion ratios. The trailing edge amplitude is maximum at the resonance which occurs at $\Pi = 0.3$ for all flexion ratios. The coincidence of the resonance frequency for all λ 's shows that the proposed scaling for the effective flexibility appropriately accounts for the effect of the flexion ratio. However, inspecting the trend of variations in A^* with Π_k reveals that the effective damping of the combined fluid-structure system increases for larger λ values. It is also worth noting that before and after resonance, higher flexion ratio foils generally experience larger trailing edge amplitude. Around the resonance the relationship is more nonlinear. For flexion ratios smaller than 0.5 the trailing edge amplitude increases with λ . This relationship is reversed for $\lambda > 0.5$.

Figure 3b shows variations in thrust and power coefficients as a function of Π_k . Unlike the trailing edge amplitude, the thrust coefficient is generally larger for smaller λ 's, except for very rigid foils where increasing λ up to 0.5 results in gain in thrust. Inspecting figure 3c shows that this gain

in thrust comes with no additional cost with regard to the power consumption. C_t rises up to its peak value at the resonance, for small λ values, and then drops quickly with further increase in flexibility. This is unlike the behavior of C_t for large λ values where the thrust plateaus before resonance and then drops with a mild slope when flexibility increases. It is worth noting that for all flexion ratios, C_t increases faster than C_p until slightly after resonance. This is reflected in Figure 3d where we show changes in the propulsive efficiency, defined as $\eta = \frac{C_t}{C_p}$, as a function of Π_k . Quick drop in thrust production after the resonance for small λ values results in a decline in the propulsive efficiency. In contrast, for large flexion ratios, η keeps increasing with flexibility for a wide range of flexibilities.

In figure 4a-b, we plotted C'_t and C'_p as the function of Π_k . When we normalized the thrust by the trailing edge velocity, the peak in the force production and power consumption disappeared implying that the peak is an artifact of the ampli-

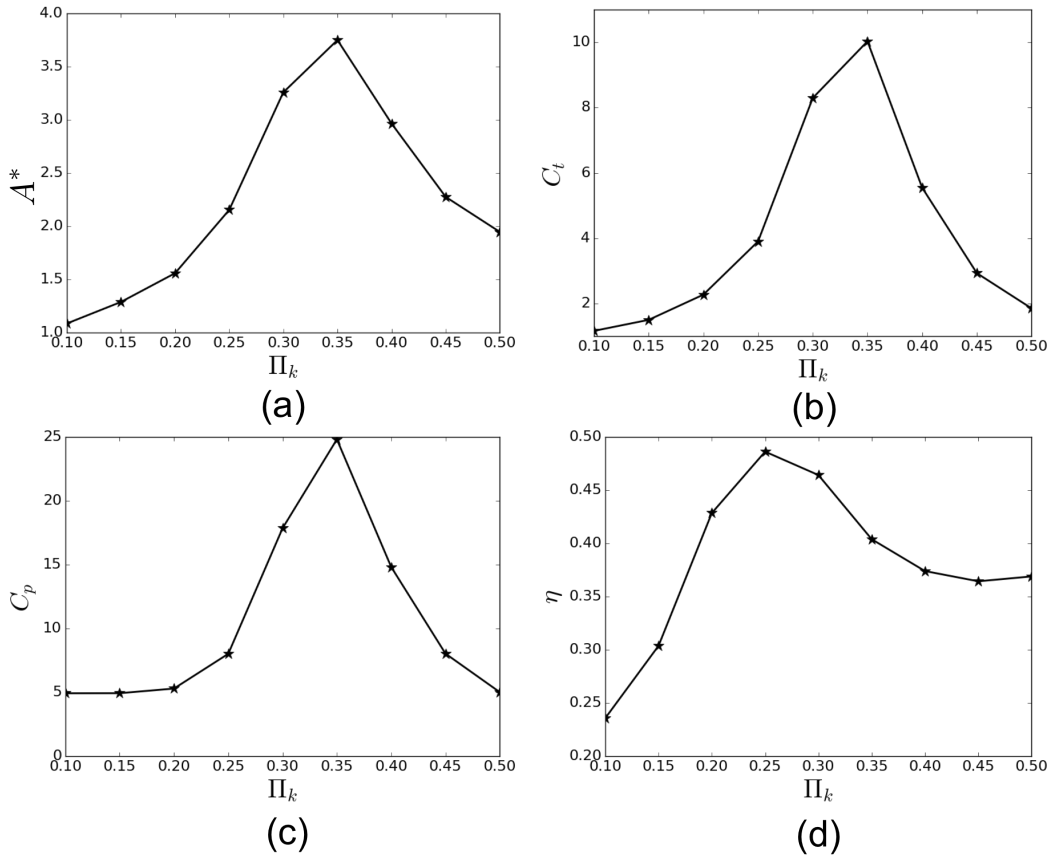


Figure 5. (a) Trailing edge amplitude, (b) thrust coefficient, (c) power coefficient, and (d) efficiency as a function of Π_k for two flexible hinge configuration.

fied trailing edge amplitude. Variations in the trailing edge amplitude are responsible for the major changes in the thrust production for $\lambda = 0$. This, however, is not the case for other λ values. The fact that the curves for different λ values do not collapse on top of one another implies that the bending pattern itself, and not only the trailing edge amplitude, play a role in the force production.

The behavior of the C_p' curves is somewhat different from that of C_t' . Before resonance, the power coefficient appear to drop quickly by increasing flexibility. After the resonance, for small λ values, the power coefficient starts to rise again. This results in a drop in efficiency which is due to a simultaneous rise in power consumption and drop in thrust production. For larger λ values, however, as flexibility increases, C_p' keeps declining where the rate of this decline decreases for large flexibilities. Thus, the rate of increase in efficiency with Π_k (figure 3d) decreases.

To summarize our findings with regard to the propulsive performance of these flexible foils, we plotted contours of C_t' and C_p' as a function of λ and Π_k in figure 4c-d. Contours of propulsive efficiency are overlaid on both figures with dotted lines. It is worth noting that the contours of efficiency line up with those of power consumption indicating that the propulsive efficiency is mostly governed by the (input) power requirement and not the thrust production. We identi-

fied three regions on these contour plots. In region 1, which contains low Π_k and low λ value foils, the thrust coefficient remains relatively constant. The propulsive efficiency can be enhanced by increasing flexibility (contours of propulsive efficiency are almost parallel to the λ -axis). In region 2, increasing either flexibility or flexion ratio benefits efficiency but compromises thrust production. In region 3, contours of power consumption, and thus propulsive efficiency, are more or less aligned with the Π_k axis, meaning that the efficiency is more sensitive to changing the flexion ratio. Thus, implying that for largely flexible foils increasing the flexion ratio can result in improved propulsive performance.

3.2 Two flexible joints

In the previous section we showed that changing the bending patterns of a pitching foil via increasing its flexion ratio is the key to improving the propulsive efficiency. However, there is a trade off to this gain since smaller flexion ratios are required for larger force production. We hypothesize that combining multiple flexible joints may be the key to gaining both in efficiency and thrust magnitude. To test our hypothesis, we repeated our numerical experiment on a pitching foil with two torsional springs located half a chord away from each other at $\lambda_1 = 0.2$ and $\lambda_2 = 0.7$. The kinematics of the leading edge was kept identical to the cases studied in the previous

section.

When multiple flexible joints are allowed not only the flexibility of the individual joint, but also the profile of flexibility distribution along the chord will affect the foil's deformations and, thus, its propulsive performance. Here, we chose a profile which maintains the effective flexibility of the foil unchanged along the chord. The spring stiffness, thus, declines quadratically with the normalized distance from the leading edge, $k \propto (\lambda - 1)^4$.

Figure 5a shows the trailing edge amplitude as a function of Π_k . A foil with two flexible joints has two resonances, which only one is captured in this figure. The resonance occurs at Π_k of 0.35 which is slightly larger than the resonance Π_k for each individual flexible joint. This suggests existence of nonlinear effects when combining the two joints. In comparison to one flexible joint configurations, the trailing edge amplitude of the present configuration reaches a higher maximum at the resonance, and drops slower afterward. The deformation of the middle element appear to be maximum at the resonance (figure 6). However, the amplitude of the motion of the last element continue to increase after the resonance decelerating the drop in the trailing edge amplitude.

Figure 5b shows the cycle-averaged thrust coefficient. Similar to the results in the previous section, the peak thrust generation occurs at the resonance but the magnitude of the peak is substantially higher. For $\Pi_k \leq 0.3$, the magnitude of C_T is similar to that of a foil with a single flexible joint at $\lambda = 0.2$ indicating that the effect of the combination of the two joints was not destructive to the thrust production capacity. All the more so, for larger flexibilities, C_T is larger than what was achieved by any of the single jointed foil configurations due to a constructive combination effect.

Unlike thrust, the power coefficient remains small for small Π_k values (figure 5c). This results in a quick rise in the propulsive efficiency of the double jointed foil, as reflected in figure 5d. Before the resonance (at $\Pi_k = 0.25$) the rate of rise in power starts to exceed that of the thrust and, thus, the propulsive efficiency declines, after reaching its peak value at $\Pi_k = 0.25$. However, after the resonance, power and thrust both drop at similar rates inhibiting the decline in the efficiency. In such a way, the two spring configuration maintains high propulsive efficiency across a wide range of flexibilities spanning on the both sides of resonance. Overall, the results of this section supports our earlier hypothesis.

4. CONCLUSIONS

It has been shown that the unsteady propulsive performance of flexible foils with a single torsional spring hinge is not only a function of their effective flexibility but also their bending patterns. Across all flexibilities tested here, increasing flexion ratio was beneficial to the efficiency while diminishing the thrust production. We showed that the combined effect of the flexibility and the flexion ratio can result in propulsive efficiencies as large as 50% or more for a purely pitching foil. This is more than 250% larger than the propulsive efficiency

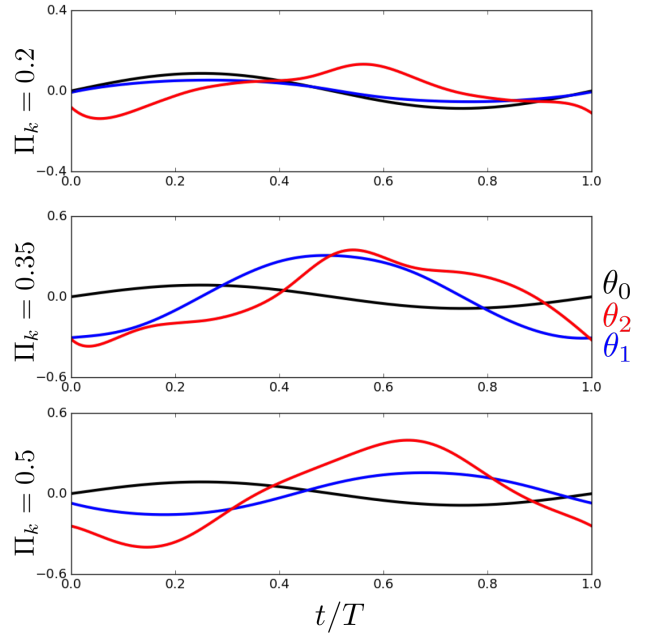


Figure 6. Change in the relative orientation of the solid elements versus time, within one cycle. Black line shows the prescribed pitching motion of the leading edge. Blue and red line, respectively, show the deflection angles of the second and the third element. The deflection angles are measured relative to the preceding element. The angles are shown for three different Π_k values of 0.1, 0.3, and 0.5. A visualization of the foil's shape at its maximum deflection is superimposed on the top of each graph.

of a rigid foil with the same leading edge kinematics.

Additionally, flexible foils with two flexible joints were examined to probe whether multiple flexible hinges could be used to attenuate the trade-off between thrust and efficiency to achieve fast and efficient swimming simultaneously. The flexibility of the joints was determined such that the effective flexibility was constant along the chord. We found that this combination of flexible joints have a constructive effect on the propulsive performance of a pitching foil with regard to both thrust and efficiency across a wide range of flexibilities.

ACKNOWLEDGMENTS

This work was funded by the Office of Naval Research under Program Director Dr B. Brizzolara, MURI Grant Number N00014-14-1-0533.

REFERENCES

- [1] T. Yao-Tsu Wu. Hydromechanics of swimming propulsion. Part 3. Swimming and optimum movements of slender fish with side fins. *Journal of Fluid Mechanics*, 46:545–568, 1971.
- [2] M. J. Lighthill. Aquatic animal propulsion of high hydromechanical efficiency. *Journal of Fluid Mechanics*, 44:265–301, 1970.

- [3] Peter A Dewey, Birgitt M Boschitsch, Keith W Moored, Howard A Stone, and Alexander J Smits. Scaling laws for the thrust production of flexible pitching panels. *Journal of Fluid Mechanics*, 732:29–46, 2013.
- [4] Hassan Masoud and Alexander Alexeev. Resonance of flexible flapping wings at low Reynolds number. *Physical Review E*, 81(5):56304, 2010.
- [5] J Katz and D Weihs. Hydrodynamic propulsion by large amplitude oscillation of an airfoil with chordwise flexibility. *Journal of Fluid Mechanics*, 88(03):485–497, 1978.
- [6] Qiang Zhu. Numerical simulation of a flapping foil with chordwise or spanwise flexibility. *AIAA journal*, 45(10):2448–2457, 2007.
- [7] Daniel B Quinn, George V Lauder, and Alexander J Smits. Maximizing the efficiency of a flexible propulsor using experimental optimization. *J. Fluid Mech*, 767:430–448, 2015.
- [8] P. A. Dewey, B. M. Boschitsch, K. W. Moored, H. A. Stone, and A. J. Smits. Scaling laws for the thrust production of flexible pitching panels. *Journal of Fluid Mechanics*, 732:29–46, 2013.
- [9] SA Combes and TL Daniel. Flexural stiffness in insect wings i. scaling and the influence of wing venation. *Journal of experimental biology*, 206(17):2979–2987, 2003.
- [10] FE Fish and GV Lauder. Passive and active flow control by swimming fishes and mammals. *Annu. Rev. Fluid Mech.*, 38:193–224, 2006.
- [11] Neil Bose, Jon Lien, and Juha Ahia. Measurements of the bodies and flukes of several cetacean species. *Proceedings of the Royal Society of London B: Biological Sciences*, 242(1305):163–173, 1990.
- [12] AK Kancharala and MK Philen. Optimal chordwise stiffness profiles of self-propelled flapping fins. *Bioinspiration & Biomimetics*, 11(5):056016, 2016.
- [13] M Nicholas J Moore. Torsional spring is the optimal flexibility arrangement for thrust production of a flapping wing. *Physics of Fluids*, 27(9):091701, 2015.
- [14] Paul Riggs, Adrian Bowyer, and Julian Vincent. Advantages of a biomimetic stiffness profile in pitching flexible fin propulsion. *Journal of Bionic Engineering*, 7(2):113–119, 2010.
- [15] J. Katz and A. Plotkin. *Low-speed aerodynamics*. Cambridge University Press, New York, NY, second edition, 2001.
- [16] D. B. Quinn, K. W. Moored, P. A. Dewey, and A. J. Smits. Unsteady propulsion near a solid boundary. *Journal of Fluid Mechanics*, 742:152–170, feb 2014.
- [17] David Joe Willis. *An Unsteady, Accelerated, High Order Panel Method with Vortex Particle Wakes*. Phd, Massachusetts Institute of Technology, 2006.
- [18] Seong Yong Wie, Seongkyu Lee, and Duck Joo Lee. Potential panel and time-marching free-wake-coupling analysis for helicopter rotor. *Journal of Aircraft*, 46(3):1030–1041, may 2009.
- [19] Yulin Pan, Xiaoxia Dong, Qiang Zhu, and Dick K. P. Yue. Boundary-element method for the prediction of performance of flapping foils with leading-edge separation. *Journal of Fluid Mechanics*, 698:446–467, apr 2012.
- [20] Robert Krasny. Desingularization of Periodic Vortex Sheet Roll-up. *Journal of Computational Physics*, 65:292–313, 1986.
- [21] Keith W Moored and Daniel B Quinn. Inviscid scaling laws of a self-propelled pitching airfoil. *arXiv preprint arXiv:1703.08225*, 2017.
- [22] Emre Akoz and Keith W Moored. Unsteady propulsion by an intermittent swimming gait. *arXiv preprint arXiv:1703.06185*, 2017.
- [23] M Nicholas J Moore. Analytical results on the role of flexibility in flapping propulsion. *Journal of Fluid Mechanics*, 757:599–612, 2014.
- [24] Daniel P Mok and WA Wall. Partitioned analysis schemes for the transient interaction of incompressible flows and nonlinear flexible structures. *Trends in computational structural mechanics, Barcelona*, 2001.
- [25] Ulrich Küttler and Wolfgang A Wall. Fixed-point fluid-structure interaction solvers with dynamic relaxation. *Computational Mechanics*, 43(1):61–72, 2008.
- [26] Iman Borazjani, Liang Ge, and Fotis Sotiropoulos. Curvilinear immersed boundary method for simulating fluid structure interaction with complex 3d rigid bodies. *Journal of Computational physics*, 227(16):7587–7620, 2008.